Experimental Analysis and 3D-Visualization of Oscillating Hollow-Conical Liquid Sheets in Quiescent Air

E. Musemic[*1], A. Rojek[1], M. Gaspar[2], F. Weichert[2], H. Müller[2] and P. Walzel[1]
[1]Department of Biochemical and Chemical Engineering and
[2]Department of Computer Science VII, Computer Graphics
[1,2]Technical University of Dortmund, D-44227 Dortmund, Germany

Abstract

This work deals with the investigation on propagating hollow-conical liquid sheets formed by a pressure swirl atomizer during the process of sheet disintegration in quiescent air. In difference to the non-invasive image based spray analysis shown by several authors, we applied an invasive experimental approach based on polymer optical waveguides. This setup allows for measurement of sheet characteristics in 2D, interpolating the data in the area between the eight sensors. The distance of these eight sensors from the nozzle orifice was graduated in small steps in order to collect sheet characteristics of the whole hyperbolical sheet. Combining the experimental results of the 2D measurements, by means of 3D reconstruction, enables visualization of the sheet behavior in 3D. Linear instability models for thinning, viscous and inviscid liquid sheets, as available from the literature, are the basis for a comparison of experimental data and predicted sheet behavior. The coexistence of longitudinal and lateral waves at lower We-numbers was confirmed, leading to the conclusion that the presence of lateral waves has to be considered.

Introduction

Swirl atomizers are found in a wide range of industrial applications, such as spray-drying, agricultural spraying, combustion of fuels and scrubbing of dust and gas. Hence, the investigation and understanding of the sheet break-up process are essential to control and improve processes based on sheet forming atomization. In this context, the knowledge of the transition from sheet to drops is of practical interest. Liquid atomization processes are too complex to allow a purely theoretical study. Therefore experimental studies are necessary to quantify various characteristics of the oscillating liquid sheet. The liquid usually enters the swirl chamber of the nozzle tangentially producing a cyclone-like internal flow, also including an air core. As soon as the liquid emerges from the nozzle orifice, it moves along straight trajectories forming a hyperbolic, often simplified as a hollow conical sheet. As the film propagates, the Kelvin-Helmholtz type of instability forms surface waves due to aero-dynamical stimulation in the ambient gas, linked to a growth of initial disturbances along the sheet streamlines. With increasing distance from the nozzle orifice, the sheet oscillation is amplified and finally causes the sheet to break. The rim contraction of broken sheet fragments leads to ligaments, which later on resolve to single droplets due to Rayleigh instability. In general, the first stage of the break-up process is described via classical linear stability theories ([1] - [3]) and drop sizes correspond mostly to existing theories based on mass balances and contraction of the sheet fragments. Newer theoretical approaches ([4], [5]) consider three-dimensional effects, such as the presence of lateral waves, which are found to have a considerable influence on the sheet disintegration process. An experimental reliable evidence of conformity to the different theoretical approaches could not yet be presented so far, because of the highly demanding task for the measuring technique. Detailed experimental data of the flow could help to verify and improve the existing theoretical models. In order to improve the understanding and the behavior of the lateral waves, they were analyzed by considering three-dimensional effects as described in [5]. Experimental investigations based on this measuring technique were presented in the past [6], when multiple optical fibers were arranged in parallel in a shape of a comb and positioned in the main flow direction of the moving sheet. The major advantage of this invasive measuring system over other non-invasive techniques is a higher temporal and spacial resolution, as well as its ability to build cost-effective multiple sensor setups. In the present work, eight of these sensors were positioned equidistantly along the perimeter allowing for measurement of sheet characteristics in 2D, interpolating the data in the area between the eight sensors. The distance of these eight sensors from the nozzle orifice was graduated in small steps in order to collect sheet characteristics of the whole hyperbolical sheet.

[*]Corresponding author, Emir.Musemic@bci.tu-dortmund.de

Experimental setup

The experimental setup consists of the measuring unit and the atomization system (Fig. 1), which allows operating at different pressures and temperatures, as well as using different nozzles. The experimental fluid is collected in an open reservoir and conveyed to the nozzle with a rotary pump in a recycle loop. The different nozzle geometries are realized by fitting different nozzle parts from a kit, so that the number of inlet ports, dimensions of the swirl chamber and outlet geometry could be changed independently. In this paper, the nozzle geometry with an orifice diameter of 15 mm has been used. Furthermore, two tangentially arranged inlet ports were fitted, each 7 mm in diameter. The dimension of the swirl chamber was 50 mm in diameter with a cone angle of 60 deg. Other nozzle geometries have not been included yet, due to the time-intensive measurements.

The measuring principle is based on the fiber technology. The measuring technique exploits the Fresnel effect on the plane fiber end to detect differences in the refractive index. In the present case, such differences are caused by the phase-change on the fibre tip, when the fiber is positioned inside a multiphase flow [7]. When light is coupled into the fiber, the intensity of the reflected light on the other end of the fiber depends on the refractive index of the fiber environment. The intensity of the reflected light can be measured with a photo diode on the remote tip of the fiber, as the fiber is transmitter and receiver at the same time. If the refractive index of the fiber core material and the fiber environment are the same, almost all coupled light is being emitted. With increasing difference in the refractive index, as e.g. in contact with air, the fraction of the reflected light on the fiber tip also increases.

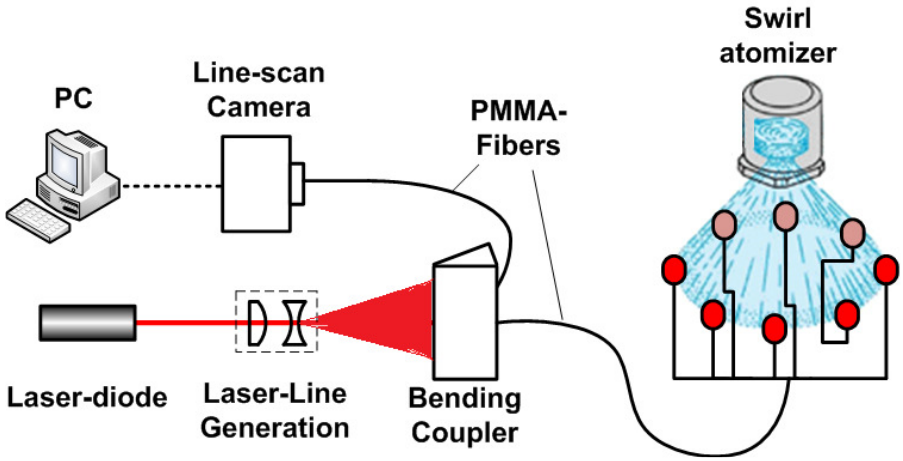

Figure 1. Principle of experimental setup

In this work, multiple fibers were bundled to a 1-dimensional array in order to detect phase-changes along a line. The fiber array consists of 440 multi-mode PMMA fibers with an outer diameter of 250 micron and a numerical aperture of 0.5. In an effort to record sheet oscillations in longitudinal as well as in lateral direction, the 1-dimensional fiber-array is divided into eight sensor-heads, arranged equidistantly along the spray perimeter, but in same distance to the nozzle orifice. Each sensor is positioned perpendicular to the flow direction of the oscillating liquid sheet, in order to detect the oscillatory sheet displacement vs. time at every single position along the spray perimeter. The distance between the sensors and the nozzle orifice was graduated in steps of 2.5 mm, which allows for taking readings along the moving path of the sheet. The light source of the measuring system is a 300 mW laser diode, with a wavelength of 660 nm. The light is focused and coupled into the fibers by using a bending coupler device [8], which consists of a metal wedge with an angle of 30 deg. The fibers are parallel oriented and bend together around the sharp edge of the wedge. A system of lenses flattens the laser beam from the diode to a light-sheet and focuses it to the sharp bend of the fibers. The coupled light is reflected at the interface between the fiber core material and the environmental fluid at the sensor end of the fiber and is recorded by a line-scan CCD camera directly mounted at the remote tip of the fibers. Thus, the fibers in this setup are acting as signal transmitter and receiver at the same time. The camera model is a DALSA Piranha 3 line scan camera with a maximum sampling rate of 33.7 kHz. Because of the limited dimensions of the camera line detector, the fiber array was mounted on the camera using a pitch converter device, converting the fiber diameter to 125 µm structures. With this setup, the motion of the oscillating sheet impinging on the sensor is recorded with a maximum spatial resolution of 250 µm and 30 µs in time. Every image consists of 7000 lines, recorded with a sampling rate of 33 kHz. The high time resolution of the

measuring system permits accurate measurement of sheet displacements at every single position along the main streamline of the moving sheet, except positions very close to the nozzle due to the sensor dimensions. Since the sensor is of invasive, the sensor tip is in permanent contact with the fluid and therefore a fast de-wetting of the fiber surface is desired. The fiber tips were therefore polished and the fiber cladding has been covered with a hydrophobic fluorine-polymer, so that the improved drain-off of polar fluids from the sensor tip leads to improved image quality of the recorded images. All experiments were performed with a water-glycerol mixture, at constant Oh-number of Oh = 0.029 (viscosity: η_L = 32 mPas, surface tension: σ = 68 mN/m). The atomization pressure was graduated in steps between $0.05 < \Delta p < 0.16$ MPa ($0.5 < \Delta p < 1.6$ bar).

Data extraction

The aim of signal extraction is to represent the imaged oscillations in terms of a set of discrete functions assigning each time step at each sensor position a sheet displacement, which can subsequently be analyzed and evaluated. The raw data are gray level images of dimension 7000×8192 pixel showing the captured intensities of the eight fiber arrays. Each column of the image represents a time step with the recorded fiber responses in its rows. Signal extraction is performed separately for each of the eight sub images using the following image processing steps. At first, the given raw image is binarized to separate the sheet contour from the background. Therefore the horizontal image gradient is computed and adaptively thresholded to identify pixel representing the position of the sheet by means of sharp gray level transitions along the time axis. The vertical image gradient is ignored, since every single fiber produces intensity gradients along the fiber array that generally can not be distinguished from sheet-position induced gradients. The binary image is filtered by means of median and morphological filters to reduce noise effects and the resulting image shows a scattered version of the signal to extract. Additional filters may be inserted into the processing queue to enhance signal accuracy. In order to meet the demand of a fast, automatic and reproducible extraction, the second step consists of approximating the signal as indicated by scattered unconnected image regions by means of a dual active contour approach ("snake") [9]. Thereby, the amount of manual interaction is reduced significantly to accelerate the image evaluation process. A snake is an energy minimizing curve guided by external constraint forces and influenced by image forces that direct it towards desired image features, such as lines and edges. The evolution of the active contour in the image is determined by minimizing the energy functional:

$$E_{snake}(v) = \int_0^1 E_{\text{int}}(v(s))ds + \int_0^1 E_{ext}(v(s))ds + \int_0^1 E_{user}(v(s))ds \quad (1)$$

in which the total Energy E_{snake} of a parametric curve v(s), with s = [0,1], is separated into three components E_{ext}, E_{int} and E_{user}, specifying the state of the curve v(s). E_{int} is defined as the strain and curvature energy of the curve:

$$E_{\text{int}}(v) = \int_0^1 a\left\|\frac{\partial}{\partial s}v(s)\right\|^2 + \int_0^1 b\left\|\frac{\partial^2}{\partial s^2}v(s)\right\|^2 ds \quad (2)$$

a and b are constants which specify the resistance of the curve against stretching and bending. In order to guide the curve to desired image features, an external energy term E_{ext} has to be supplied. The last term of Eq. (1) may be used for imposing user-controlled constrains of the curve [9]. In the present approach, an additional force induces the two curves to move towards each other. Finally, the solution of partial differential equations associated with the active contour is computed by a finite difference scheme [10]. The dual active contour is initialised at the top (curve v_o) and bottom (curve v_u) of the image and approximation of the signal is stopped when the distance between v_o and v_u reaches a local minimum. An intermediate signal is calculated from the final curves v_o and v_u to reduce artifacts and dependence on direction of approximation. Following this procedure, all curves can be sampled and plotted as a discrete time/space-plot, which is the basis of further data evaluation.

Results and Discussion

The sensor arrangement allows for a quite detailed view of the sheet behavior, in longitudinal as well as in lateral direction. In general, sheet oscillation amplitudes are seen to grow along distances, regardless of weather lateral-wave modes are present. The arrangement of the eight fiber sensors, which are positioned equidistantly along the hollow cone sheet in lateral direction, enables lateral oscillation analysis. Sheet oscillations in both directions of the spray hollow cone, longitudinal and lateral, and at different We-numbers are shown in Fig 2. The plot shows the

relative sheet oscillation displacement against time and the position in circumferential direction of the spray cone. In all cases the shown total time period is equivalent 0.21 s and the areas between the one-dimensional sensors are being interpolated. The distance between the eight fiber sensors along the x-axis is in a range of 25-35 cm, depending on the spray angle at each setting. The resulting spatial resolution in lateral direction is in range of 3,2-4,4 cm. Therefore, only long wave oscillations in lateral direction may be detected accurately.

For the time being, a Fourier- or Wavelet based frequency analysis in circumferential direction has not yet been implemented in the evaluation software, so far. Therefore, only a qualitative analysis is presented. In the first case (Fig. 2a), i.e. at lower We-numbers (We = 8932.5), a formation of long lateral waves can be observed. The Wavelength of the lateral waves is approximately 130 mm, resulting in an oscillation frequency of 31 Hz, considering the sheet velocity obtained in [6]. Increasing the We-number (We = 17507.7) (Fig. 2b) the formation of even longer lateral waves can be observed. In this case, the wave length is approximately 195 mm, but resulting in slightly increased frequency of 43 Hz because of higher sheet velocity at this setting. Increasing the We-number even higher (We = 23587.4) (Fig. 2c) leads to longitudinal waves and no significant appearance of lateral waves. In summary, increasing the We-number results in a smooth transition of oscillation modes with lateral waves to those with almost only longitudinal (along trajectories) wave pattern.

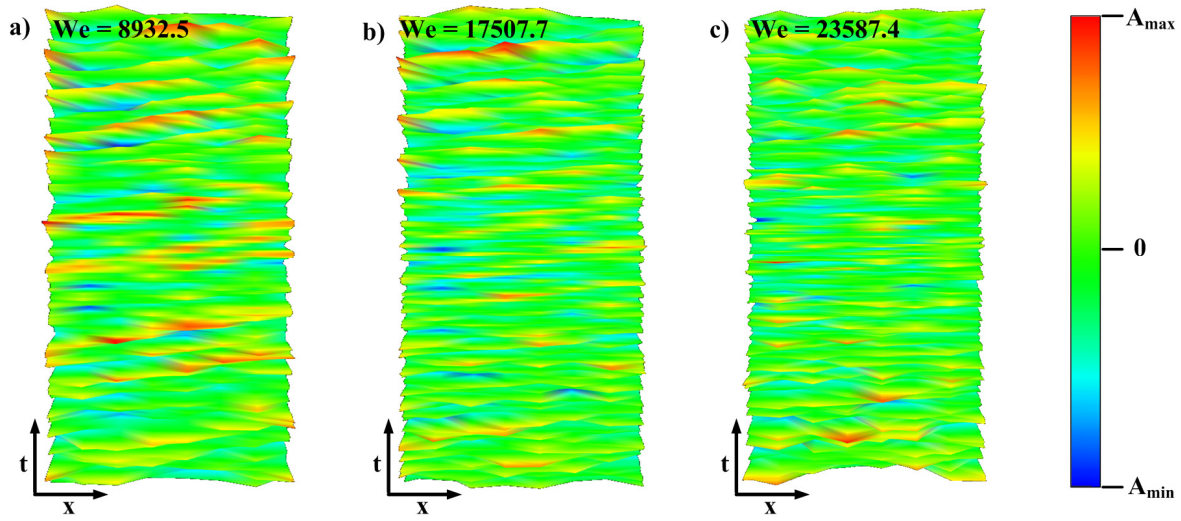

Figure 2. Visualization of sheet displacement in 2D+t at different operating conditions:
a) Δp = 0.05 MPa, We = 8932.5; b) Δp = 0.1 MPa, We = 17507.7; c) Δp = 0.16 MPa, We = 30571.5

Tharakan and Ramamurthi [5] predict a similar behavior of oscillating sheets. It was shown, that implementing the presence of lateral waves into their model improved the accuracy of droplet distribution predictions validated with experimentally verified drop sizes. However, an experimental validation of the coexistence of longitudinal and lateral wave pattern at lower We-numbers has not been shown yet. Since nonlinear growth rates can be significantly larger than those predicted by linear theory, as shown by Mehring and Sirignano [4], the experimental quantification of sheet oscillation frequencies and amplitudes, including the oscillations in lateral direction, may help to improve the existing calculation models. In general, higher growth rates of sheet disturbances lead to an earlier sheet breakup by trend and therefore a different drop size distribution may occur.

In addition to the measurements and visualizations in 2D+t, the experimental data at the vertical distances between the nozzle orifice and the sheet break-up location have been combined to a 3D-plot in order to visualize the oscillation characteristics on the whole sheet. Fig. 3 shows an exemplary 3D-Plot for various sheet oscillation parameters at constant atomizing pressure of 0.13 MPa within a distance range between 30 and 80 mm. The first plot (Fig. 3a) shows the continuity of the recorded oscillation signal. If there is some discontinuity in the recorded signal, i.e. when the sheet is breaking up, the active contours will interpenetrate. This feature was used to define the position of the sheet breakup along the main flow direction. Close to the nozzle, the liquid sheet is almost continuous. As the sheet moves away from the orifice, the continuity of the sheet decreases due to hole formations till break-up. In the present case, areas where the hole formations are indicating the beginning of sheet break-up, can be approxi-

mately located in the middle of the observed area, i.e. at 55 mm distance. Because of a smooth transition between continuous sheet and sheet breakup, the break-up location has to be defined on available sheet characteristics, such as the signal continuity. In previous investigations [6] the distance of sheet break-up was defined at the place, where the signal-continuity is 50%. The second plot (Fig. 3b) shows the distribution of oscillation frequencies with the highest energy content, i.e. the highest amplitudes. It can be obtained, that the frequency distribution is almost homogeneous with a dominating frequency of about 95 Hz, although there is a slight decrease of dominating frequency in the main flow direction of the sheet. This slight decrease might be caused by the deceleration of the sheet in the ambient gas, which was observed in [6] and [11]. In Fig. 3c the corresponding maximum amplitudes of the dominating frequencies are shown. The increase in amplitude is almost linear with increasing distance from the nozzle orifice. This behavior was observed with all operating conditions, whereas the dominating frequencies and the corresponding amplitudes increased with higher atomization pressures. Since the sheet oscillations are directly linked to the resulting drop sizes, such experimental data might improve existing models with the aim to predict drop sizes more accurately. In Fig. 3d the spatial distribution of mean oscillation frequencies on the sheet is shown. The plot indicates, that there are much higher frequencies existent than the measured dominating frequencies, including a slightly decrease along the liquid flow direction. In the present, it is quite unclear which influence these high frequency oscillations have on the sheet disintegration process, since they appear with relative small amplitudes. Further investigations have to be done on this topic, to improve the understanding of the primary sheet break-up into ligaments. In addition, the visualization indicates no observable influence of the dual tangential inlets on the shape of the spray cone as well as on the oscillation indicating a very uniform swirl flow, which is also shown in [12].

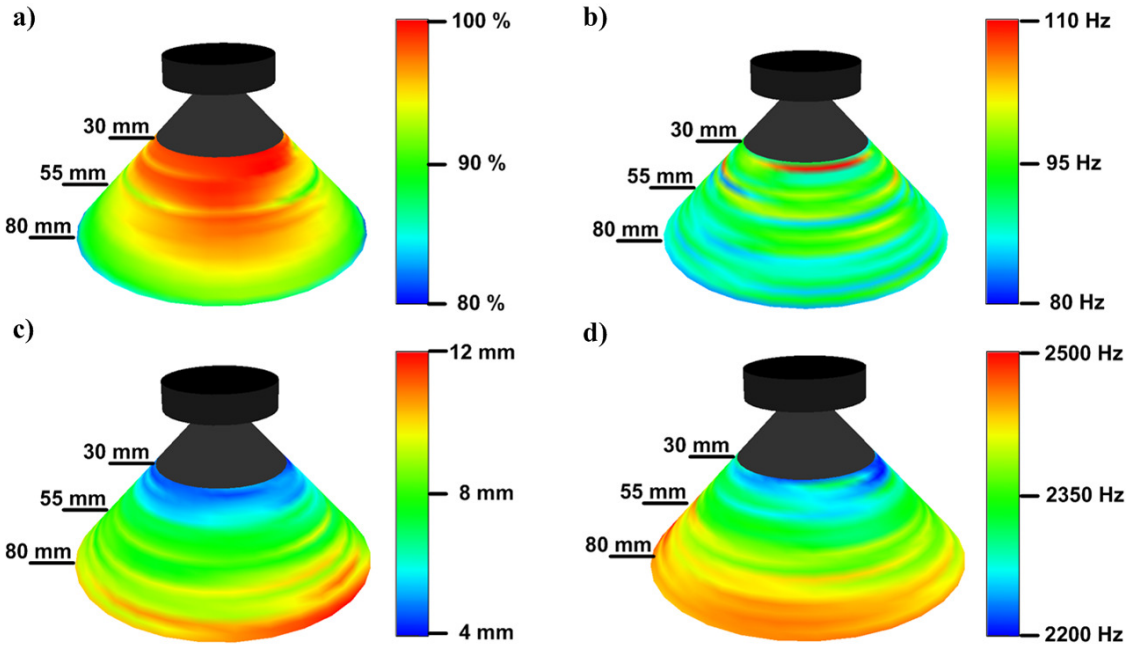

Figure 3. Visualization of sheet characteristics in 3D (We = 23587.4, Oh = 0.029): a) Sheet continuity; b) Oscillation frequency of maximum amplitude; c) Maximum Amplitude; d) Mean oscillation frequency

Conclusions

The investigations have shown different characteristics in the growth of aerodynamic waves, depending on the operating conditions. Within the range examined, the frequency analysis of the sheet oscillation shows dominating oscillation frequencies at all flow conditions within the range of $70 < f < 150$ Hz. Higher frequencies (> 150 Hz) with higher intensities or amplitudes were not detected. In addition, the visualization indicates no visible influence of the dual tangential inlets on the shape of the spray cone as well as on the oscillation characteristics. The coexistence of longitudinal and lateral waves at lower We-numbers was shown experimentally, leading to the conclusion that lateral waves are not negligible and therefore the theoretical research should primarily focus on improvement of existing non-linear models.

Nomenclature

Symbol	Quantity	SI Unit
a	Snake parameter 1 (stretching)	-
b	Snake parameter 2 (bending)	-
D	Nozzle orifice diameter	m
E_{snake}	Resulting snake energy	-
E_{ext}	External snake energy	-
E_{int}	Internal snake energy	-
E_{user}	User defined snake energy	-
f	Oscillation frequency	1/s
v_{eff}	Effective sheet velocity (absolute value)	m/s
v(s)	Parametric curve	-
Δp	Pressure gradient	Pa
η_L	Dynamic liquid viscosity	kg/(m·s)
ρ_L	Liquid density	kg/m³
σ	Surface tension	kg/s²
λ	Oscillation wavelength	m
$Oh = \eta_L/(\rho_L \sigma D)^{0.5}$	Ohnesorge-number	-
$We = (\rho_L v_{eff}^2 D)/ \eta_L$	Weber-number	-

References

1. Squire, S.B., Investigation of the Instability of a Moving Liquid Film, *Brit. J. Appl. Phys.*, 4:1967-1969 (1953)
2. N. Dombrowski, N., and W. R. Johns, The Aerodynamic Instability and Disintegration of Viscous Liquid Sheets, *Chem. Eng. Sci.*, vol.18, pp. 203-214, 1963
3. Senecal at all, Modeling High-Speed Viscous Liquid Sheet Atomizationm, *Int. J. Multipase Flow*, 25:1073-1097 (1999)
4. Mehring, C., and Sirignano, W.A., Capillary Stability Of Modulated Swirling Liquid Sheets, *Atomization and Sprays*, 14:397-436 (2005)
5. Tharakan, T.J., and Ramamurthi, K., Growth of Longitudinal Waves in Plane Liquid Sheets Having Lateral Waves Modes When Exposed to Two Gas Streams of Unequal Velocities, *Atomization and Sprays*, 15:181-200 (2005)
6. Musemic, E., Walzel, P., Gasper, M., and Weichert, F., Analysis of Multiphase Flow during the Process of Sheet Disintegration at Hollow Cone Nozzles using Multiple One-Dimensional Fibre-Sensors, *ILASS-Europe 2008*, Como, Italy, 8-10 Sep. 2008
7. Landwehr, F., Wiggers, H., and Walzel, P., A New Technique for Multi-Phase Spray Analysis at High Loads, *ILASS-Europe 2001*, Zurich, 2-6 Sep., 2001
8. Landwehr, F., Feggeler, D., Walzel, P., Weichert, F., Schröter, S. and Müller, H., A Fibre Sensor Based Frequency Analysis of Surface Waves at Hollow Cone Nozzles, *Experiments in Fluids*, 40:523-532 (2005)
9. Kass, M., Witkin A., and Terzopoulos, D., Snakes: Active Contour Models, *Int. J. of Computer Vision*, 1:321-331 (1988)
10. Press, W., Teukolsky, S., Vetterling W. and Flannery, B., *Numerical Recipes in C. 2nd edition*, Cambridge University Press, 1992
11. Lienemann, H., Shrimpton, J., and Fernandes, E., A Study on the Aerodynamic Instability of Attenuating Liquid Sheets, *Experiments in Fluids*, 42:241-258 (2007)
12. Broll, P., and Walzel, P., PIV Measurements in Pressure Swirl Atomizers, *ILASS-Europe 2001*, Zurich, 2-6 Sep. 2001